Applied Geochemistry 128 (2021) 104957

Contents lists available at ScienceDirect

Applied Geochemistry

journal homepage: http://www.elsevier.com/locate/apgeochem

# Interaction of aqueous antimony(III) with synthetic ferrous sulfide

Dongli Li [a], Guoping Zhang [a,*], Qingyun Wang [a,b], Shirong Liu [a], Chao Ma [a,b], Jingjing Chen [a,b], Fengjuan Liu [c]

[a] State Key Laboratory of Environmental Geochemistry, Institute of Geochemistry, Chinese Academy of Sciences, Guiyang, 550081, China
[b] University of Chinese Academy of Sciences, Beijing, 100049, China
[c] School of Geography and Tourism, Guizhou Education University, Guiyang, 550018, China

ARTICLE INFO

Editorial handling by Dr. Z Zimeng Wang

*Keywords:*
Antimony
FeS
Interaction
Mechanism

ABSTRACT

Ferrous sulfide (FeS) is an important carrier for metal(loid)s in anoxic environments, but the effect of FeS on the behavior of Sb is poorly understood. This work investigated the interaction of Sb(III) with FeS under anoxic condition. FeS was synthesized and both equilibrium and kinetic experiments on the interaction of Sb(III) with synthesized FeS were conducted at various pH values. The final solid phases were examined by SEM, XRD, TEM, and XPS. The results showed that the uptake of Sb(III) by FeS increased as pH decreased. The kinetic experiment at pH 5 obviously showed that the temporal decrease of $Sb(III)_{aq}$ coincide with the partial dissolution of FeS. In contrast, both the concentrations of $Sb(III)_{aq}$ and FeS in the kinetic experiment at pH 9 did not vary with time. The examination of the solid phases revealed the formation of amorphous $Sb_2S_3$ in the experiments at pH 5 and 7.5. Different mechanisms were suggested to affect the interaction of Sb(III) with FeS under acidic and alkaline conditions. At pH 9, adsorption dominated in the interaction. The decrease of $Sb(III)_{aq}$ and the concomitant partial dissolution of FeS at pH 5 indicated the replacement of FeS by $Sb_2S_3$, which was more significant at lower pH. The replacement of FeS by $Sb_2S_3$ was a relatively slow process compared to the acidic dissolution of FeS. The result of this study helps understand the mobility of Sb in anoxic environments and may favor the remediation of Sb contamination by the use of FeS.

## 1. Introduction

Antimony is a toxic and carcinogenic metalloid of global concern (Amarasiriwardena and Wu, 2011; Kulp et al., 2014). It is considered as pollutants of priority interest by the European Union and the United States Environmental Protection Agency (Ungureanu et al., 2015). In the environmental systems, Sb can display in four oxidation states (−3, 0, +3, and +5) but is mostly found in two oxidation states (+3 and + 5). It usually occurs as $Sb(OH)_6^-$ (Sb(V)) in relatively oxic environments or $Sb(OH)_3$ (Sb(III)) in anoxic environments (Filella et al., 2002a, 2002b; Wilson et al., 2010).

Antimony is of growing interest to industry. A significant input of Sb into the environment can result from some industrial processes, such as mining/smelting and the manufacture of alloys, semiconductors, fire retardants, glass, and polyethylene terephthalate (Filella et al., 2002a; He et al., 2012).

In terrestrial environment, ubiquitous iron hydro(oxides) such as ferrihydrite, goethite, and hematite are recognized as the primary solid phases for sequestration of metal(loid)s. In a creek draining an abandoned antimony mine, iron oxides are the main carrier phases for Sb in the suspended particulate matter (Casiot et al., 2007). In a river adjacent to the Hillgrove Sb-bearing deposits, Australia, attenuation of Sb occurs by deposition onto amorphous iron oxyhydroxides which can contain >10% of Sb (Ashley et al., 2003). In anoxic environments, reductive transformation of iron hydro(oxides) occurs due to microorganisms or reducing agents and amorphous FeS is typically the initial iron sulfide phase to form (Wolthers et al., 2005a; Burton et al., 2011, 2019). The naturally formed FeS can serve as a major sink of metal(loid)s in sediment or groundwater and significantly affect the mobility of metal(loid)s (Wolthers et al., 2003, 2005b; Han et al., 2011). For example, in relatively reducing sediment, Sb associated with iron oxides may undergone post-depositional transformation and redistribute via precipitation as sulfide or sorption to sulfide surfaces (Coles et al., 2000; Fawcett and Jamieson, 2010). It has also been reported that FeS may be abundant in acid sulfate soil environments and significantly affect the mobility of Sb (Tighe et al., 2013; Karimian et al., 2018). Additionally,

* Corresponding author.
*E-mail address:* zhangguoping@vip.gyig.ac.cn (G. Zhang).

https://doi.org/10.1016/j.apgeochem.2021.104957
Received 16 January 2021; Received in revised form 28 March 2021; Accepted 2 April 2021
Available online 6 April 2021

FeS can be applied for remediation of groundwater and soil contaminated with metal(loid)s because FeS has excellent adsorbent properties to some metal(loid)s (Gong et al., 2016; Chen et al., 2019). Therefore, the interaction between FeS and metalloids is of growing concern. The adsorption and precipitation of As by FeS have been reported in some previous studies (Wolthers et al., 2005b; Han et al., 2011; Xie et al., 2016), but the interaction of Sb and FeS has been less studied. Recently, Han et al. (2018) investigated the interaction of Sb(III) with FeS under anoxic condition in a laboratory research. However, details of the interaction between Sb(III) and FeS are far from being well understood. Particularly, Sb has a high affinity to sulfur (Filella et al., 2002a) and can compete strongly with Fe(II) on the surface of FeS. We hypothesized that this competition can significantly affect the behavior of Sb in anoxic environments. To test this, we reacted Sb(III) with synthesized FeS with emphasis on the competition between Sb(III) and Fe(II) in the system. Knowledge about the interaction of Sb(III) with FeS would be important to understand the mobility of Sb in anoxic environments.

## 2. Materials and methods

Deionized water (DW) (resistivity: 18.2 MΩ cm) was prepared with a Milli-Q system (Millipore, Bedford, MA, USA). Deoxygenated deionized water (DDW) was prepared by sparging DW with high-purity $N_2$ (99.99%). Potassium antimonyl tartrate sesquihydrate (>99% purity) was purchased from Acros Organics Inc. (New Jersey, USA). Ferrous sulfate heptahydrate ($FeSO_4{\cdot}7H_2O$), sodium sulfide nonahydrate ($Na_2S{\cdot}9H_2O$) and other chemicals were of analytical grade. All solutions were prepared with DDW. Stock solutions of Sb(III) (500 mg/L), S(-II) (0.2 M), and Fe(II) (0.2 M) were prepared by dissolving potassium antimonyl tartrate sesquihydrate, sodium sulfide nonahydrate, and ferrous sulfate heptahydrate in DDW, respectively.

The synthesis of FeS and the preparation of Sb(III) uptake by FeS were conducted in an anaerobic chamber (Model 855-ACB, PLAS-LANS, CO, USA) at an atmospheric composition of 95% Ar/5% H2. The residual oxygen inside the chamber was removed by Pd catalysts, resulting in an oxygen concentration below 1 ppm.

Amorphous FeS was synthesized by mixing a ferrous sulfate solution with a sodium sulfide solution as described by Jeong et al. (2008). In brief, 0.2 M Fe(II) solution and 0.2 M S(-II) solution (V:V = 1:1) were mixed and black amorphous FeS precipitates quickly formed. The freshly precipitated FeS was used for the experiments on the dissolution of FeS and the interaction of Sb(III) with FeS. After the precipitation of FeS, sodium chloride was added to obtain 0.1 M NaCl as a background ionic medium. Then, the stock solution of Sb(III) was added into the FeS suspension to obtain a preset initial Sb(III) concentration. Preliminary tests showed that addition of sodium tartrate did not affect the dissolution of FeS. The pH of the initial suspensions was adjusted by the addition of 0.1 M HCl and 0.1 M NaOH. The pH of the suspensions got stabilized within approximately 20 min. The initial volume of the solution was adjusted through the addition of DDW. Batch experiments were conducted in polyethylene vials. The vials were put on a shaker.

Equilibrium experiments on the dissolution of FeS and the uptake of Sb(III) by FeS as a function of pH as well as kinetic experiments on the interaction of Sb(III) with FeS (over a period of 1,440 min) were carried out. The reaction time was 3 h for the dissolution of FeS as a function of pH and 24 h for the interaction of Sb(III) with FeS. The solution was sampled at the end of equilibrium experiments or at appropriate intervals of the kinetic experiments. After collection, the solution sample was immediately filtered using a cellulose membrane (0.22 μm pore size) for the determination of dissolved ions.

All experiments were carried out at room temperature (20–25 °C) in triplicate and the mean data were reported. Some other details for each experiment were later given in the caption of figures.

### 2.1. Analyses and solid characterization

The pH of the solution was measured with a Denver UB-7 pH-meter. Fe(II) concentration was measured by a 1,10-phenanthroline spectrophotometric method (APHA, 1998). The precision of the measurement of Fe(II) in the solution was better than 3%. The solid FeS concentration was calculated as the difference between the concentrations of the initial FeS and the dissolved Fe(II). The concentration of Sb(III) was determined by hydride generation- atomic fluorescence spectrometry (HG-AFS) (AFS-2202E, Haiguang Instruments Corp., Beijing, China) following a method from Fu et al. (2016). The limit of detection for Sb (III) based on 11 replicate analyses was 0.05 μg/L, and the relative standard deviation was 0.6%.

The morphology of the synthesized FeS was examined by a scanning electron microscope equipped with an energy dispersive spectrometer (SEM-EDS, Model JSM-6460LV, JEOL, Japan). The mineralogy of the solid phases after interaction was characterized by X-ray diffractometer (Empyrean, PANanalytical Co., The Netherlands) using a Cu tube and a scanning range from 4° to 60° with a step size of 0.03° and 8 s/step measuring time. The solid phases after the interaction were also examined by a field emission transmission electron microscope (Tecnai G2 F20 S-TWIN, FEI Inc., USA), and an X-ray photoelectron spectroscopy (XPS, ESCALAB 250Xi, Thermo Fisher Scientific, Inc, USA). In the TEM-EDS analysis, semi-quantitative atomic percentages were calculated based on the signals of Fe, Sb, and S of the sample and matrix corrections were made in the software. XPS is an important surface-sensitive technique with an analytical depth of about 0–10 nm. Here, XPS was used to determine the binding of Sb on the solid phases.

## 3. Results and discussion

An SEM image of the freshly synthesized mackinawite (Fig. 1) shows that the FeS was clusters of very fine grains. Similarly, it was noted that FeS synthesized using this procedure was extremely fine-grained and aggregated, and was therefore difficult to characterize (Csakberenyi-Malasics et al., 2012). Amorphous FeS initially formed in anoxic environments is thought to be nanocrystalline mackinawite (Rickard et al., 1995), which tends to agglomerate rapidly. A wide range of the particle size of precipitated FeS have been given in literature. For example, some previous studies reported the particle size of precipitated FeS synthesized using the same procedure to be 4.2 nm (Wolthers et al., 2003), 3–11 nm (Ohfuji and Rickard, 2006), and 3.5 nm (Jeong et al., 2008).

### 3.1. FeS solubility

The effect of pH on the dissolution of FeS was examined in the pH

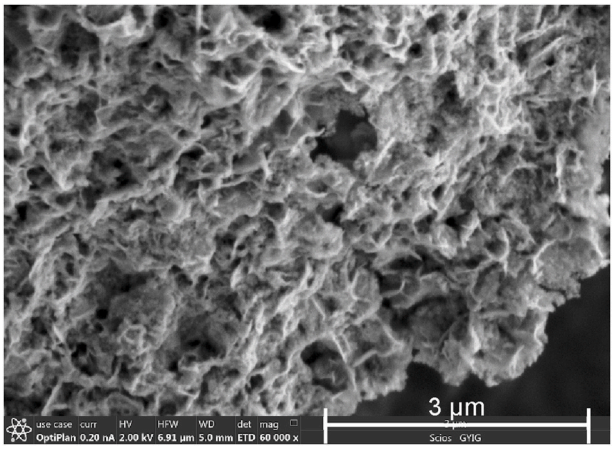


**Fig. 1.** SEM image of the precipitates of FeS.

range 3–9.5 (Fig. 2). The dissolution of FeS was found to be highly dependent of pH. When pH decreased, the dissolution of FeS increased significantly. For example, only 1.4% of FeS dissolved at pH 9.5, whereas approximately 70% of FeS dissolved at pH 5. Similarly, the high dissolution of FeS at acidic pH has also been observed in previous studies (Wolthers et al., 2005b; Han et al., 2018). The dissolution of FeS can be described as follows:

$$FeS_{(s)} + 2\ H^{+} \rightarrow Fe^{2+} + H_2S \quad (1)$$

In this reaction the proton competes for S(-II) and forms $H_2S$ (or $HS^-$), resulting in the increase of FeS dissolution at low pH.

### 3.2. Batch interaction experiments

The result of equilibrium experiments on the interaction of Sb(III) with FeS at pH 5 to 9 is shown in Fig. 3. In the control experiment (Sb(III) only) at each pH, the $Sb(III)_{aq}$ concentration did not show deviation from the initial value of 20 mg/L, indicating that the $Sb(III)_{aq}$ was not affected by any processes (e.g, Sb precipitation) over this pH range. In the experiments (FeS + Sb(III)), the $Sb(III)_{aq}$ decreased with decreasing pH. This contrast indicates that the concentration of $Sb(III)_{aq}$ was only affected by the interaction of Sb(III) with FeS and this interaction was pH dependent. The concentration of $Sb(III)_{aq}$ differed markedly between experiments under acidic and alkaline conditions. In the experiment at pH 5, the residual $Sb(III)_{aq}$ concentration was only 3.2 mg/L (equivalent to 84% decrease) compared to 15.5 mg/L (equivalent to 22.5% decrease) in the experiment at pH 9. This striking contrast possibly indicates that different mechanisms were responsible for the uptake of Sb (III) by FeS under acidic and alkaline conditions.

Kinetic experiments on the uptake of Sb(III) by FeS were conducted at pH 5, 7.5, and 9, respectively. The temporal variation of FeS and Sb $(III)_{aq}$ concentrations in the experiments is shown in Fig. 4. The variation of FeS concentration without addition of Sb(III) is also shown in this figure. In the control experiments (FeS only) at pH 5, 7.5, and 9, the FeS concentration was 20, 35, and 40 mg/L at the beginning of the experiment and was basically steady thereafter (Fig. 4a and b and c). Taking into account the FeS was initially added at a concentration of 40 mg/L in each experiment, the initial dissolution of FeS was negligible at pH 9 but was more significant at pH 5 and 7.5. The initial dissolution of FeS in the experiments at pH 5 and 7.5 is consistent with the above-mentioned result that the dissolution of FeS was more significant at lower pH. The initial drop of the concentration of FeS at pH 5 and 7.5 indicates that the acidic dissolution of FeS (reaction (1)) is a rapid and efficient process.

In the control experiments (FeS only) at pH 5, 7.5 and 9, the basically

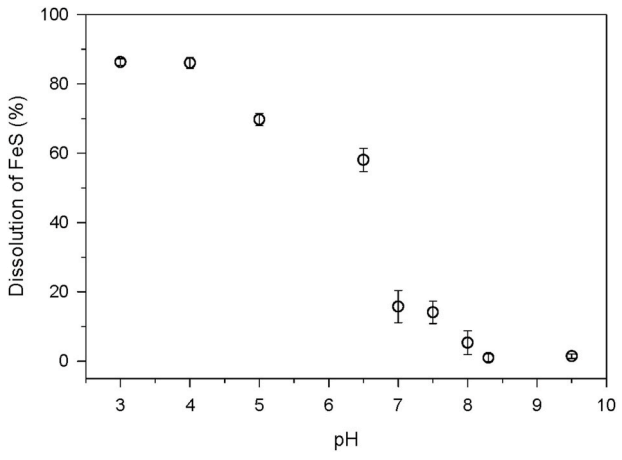


**Fig. 2.** Dissolution of FeS as a function of pH (initial FeS concentration: 40 mg/L; interaction time: 3 h).

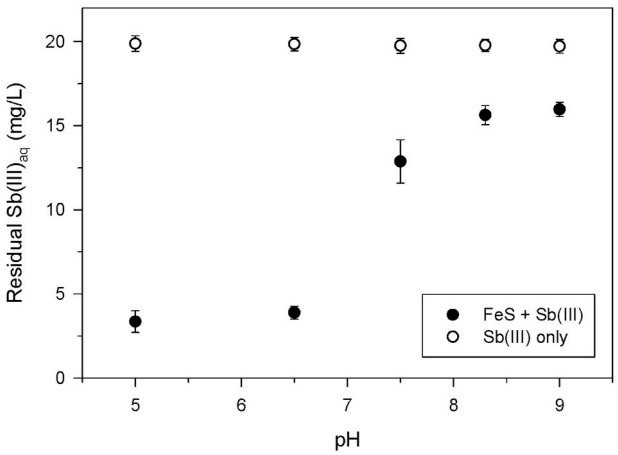


**Fig. 3.** Uptake of Sb(III) by FeS as a function of pH (initial FeS concentration: 40 mg/L; initial Sb(III) concentration: 20 mg/L; interaction time: 24 h).

steady concentration of FeS after the beginning of the experiment (Fig. 4a and b, and c) indicates that, without addition of Sb(III), the solid FeS did not further dissolve. In the presence of Sb(III), the temporal variation of FeS concentration at various pH values differed significantly. In the kinetic experiment (FeS + Sb(III)) at pH 5, the FeS concentration further decreased from 20 mg/L at the beginning to 11.4 mg/L at the end, indicating that FeS further dissolved after the addition of Sb (III). This indicates that the addition of Sb(III) resulted in gradual dissolution of a fraction of FeS. Moreover, the gradual decrease of FeS and $Sb(III)_{aq}$ over this period reflected a relatively slow interaction between Sb(III) and FeS particles, which contrasted to the rapid acidic dissolution of FeS (reaction (1)). In the kinetic experiments of both (FeS + Sb(III)) and (FeS only) at pH 9, the FeS concentration was identical (approximately 40 mg/L) at the beginning of the experiment and was basically steady thereafter (Fig. 4c). This indicates that, even in the presence of Sb(III), no significant dissolution of FeS occurred at pH 9. In the kinetic experiment (FeS + Sb(III)) at pH 7.5, the concentrations of both FeS and $Sb(III)_{aq}$ were between the kinetic experiments at pH 5 and 9 (Fig. 4). It can be postulated that the addition of Sb(III) at pH 7.5 also resulted in some dissolution of FeS. However, the dissolution of FeS at pH 7.5 was notably weaker than that at pH 5.

### 3.3. Characterization of the solid phases after interaction

The solid phases of the kinetic experiments (FeS + Sb(III)) were examined by TEM-EDS (Fig. 5). In the solid phase of the kinetic experiment (FeS + Sb(III)) at pH 5, precipitates of $Sb_2S_3$ were found as aggregates that coexisted with FeS particles (Fig. 5a). EDS analysis of the focus area of the aggregates showed strong signals of S, Sb, and Fe, and the semi-quantitative atomic percentages of Fe, Sb, and S were 4.5%, 33.8%, and 61.7%, respectively (Fig. 5d). This corresponds to the composition of a mixture with $Sb_2S_3$: FeS = 4:1 (molar ratio). In the solid phase of the kinetic experiment (FeS + Sb(III)) at pH 7.5, precipitates of $Sb_2S_3$ were also found (Fig. 5b) but at a markedly lower frequency. The semi-quantitative atomic percentages of Fe, Sb, and S of the focus area were 9.6%, 32.6%, and 57.8% (Fig. 5e), which corresponds to the composition of a mixture with $Sb_2S_3$: FeS = 5:3 (molar ratio). However, no precipitates of $Sb_2S_3$ were found in the solid phase of the kinetic experiment (FeS + Sb(III)) at pH 9. This indicates that, in the interaction of Sb(III) with FeS, the formation of $Sb_2S_3$ was not significant at high pH.

The solid phases of the kinetic experiment (FeS + Sb(III)) at pH 5 were examined by XRD. The solid phases showed a very similar XRD pattern to that of pure FeS (Fig. 6). Although the TEM examination showed the occurrence of $Sb_2S_3$ precipitates in the solid phases, no signals concerning Sb sulfides were observed in the XRD analysis.

Fig. 7 shows the XPS Sb-3d spectra of the solid phases of the

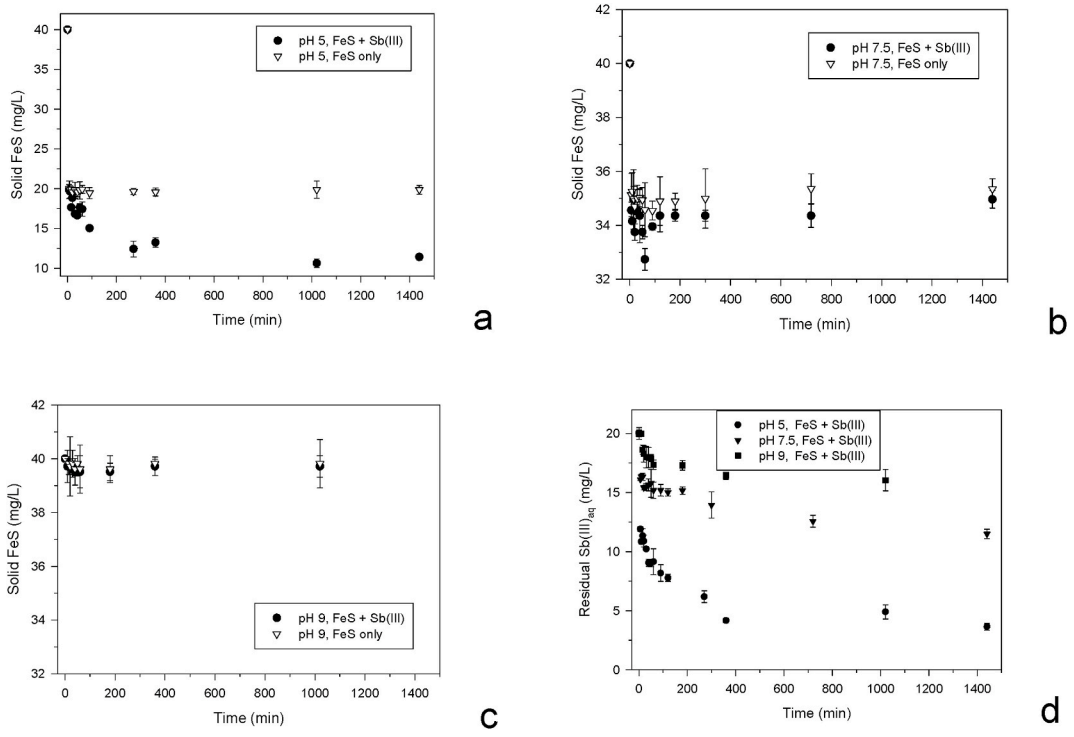


**Fig. 4.** Evolution of FeS and Sb(III) concentrations over time (initial FeS concentration: 40 mg/L; initial Sb(III) concentration: 20 mg/L).

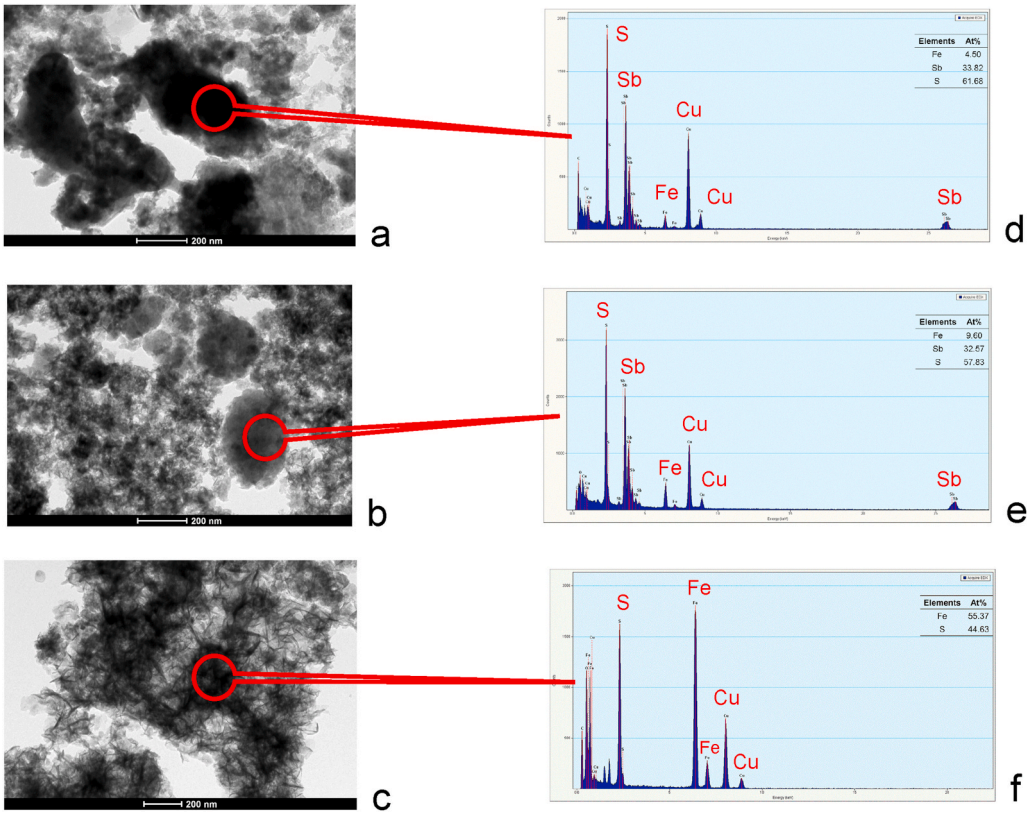


**Fig. 5.** TEM image and EDS spectrum of the solids after interaction (a: pH 5; b: pH 7.5; c: pH 9) (The signal of Cu originated from the copper support for the sample).

experiments (FeS + Sb(III)) at pH 5, 7.5, and 9. The chemical bonds of both Sb(III)–S and Sb(III)–O were found in all the solid samples. The signal of Sb(III)–S can originate from the precipitates of $Sb_2S_3$ as well as the binding of Sb(III) to sulfide functional group $\equiv SH^0$ (Bebie et al., 1998) on the surface of FeS particles. The signal of Sb(III)–S was strongest in the pH 5 sample while it was weakest in the pH 9 sample. This is consistent with the result that the formation of $Sb_2S_3$ was more significant at lower pH. The occurrence of chemical bond Sb(III)–O is

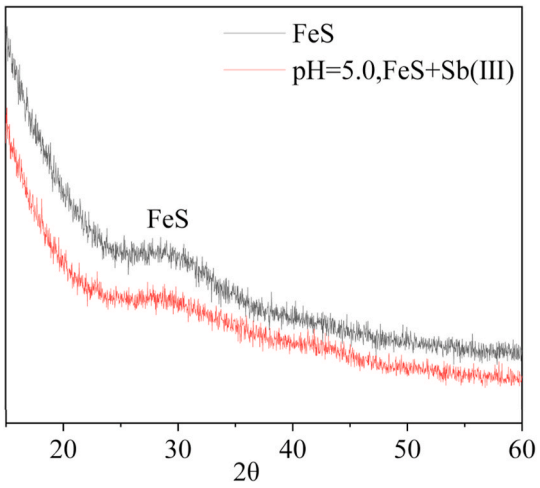


**Fig. 6.** Comparison of the XRD pattern of the solid phase with that of pure FeS.

considered corresponding to the adsorption of $Sb(OH)_3$ on the surface of FeS. The strong Sb(III)–O signal in all the three samples indicates that adsorption may contribute to the interaction of Sb(III) with FeS under both acidic and alkaline conditions. The adsorption of Sb(III) is further elucidated at the end of next section.

### 3.4. The uptake of Sb(III) by FeS

Under anoxic conditions, aqueous Sb(III) is predominantly present as $Sb(OH)_3$ (Filella et al., 2002b). When sulfide is present, Sb(III) can react with sulfide and form precipitates of $Sb_2S_3$ (Wang et al., 2013; Zhang et al., 2016; Han et al., 2018).

$$2\ Sb(OH)_3 + 3\ H_2S \rightarrow Sb_2S_{3(s)} + 6\ H_2O \quad (2)$$

In this reaction, $H_2S$ represents the sum of sulfide species in solution that consist of $H_2S$, $HS^-$, and $S^{2-}$.

The solubility product ($K_{sp}$) is a key factor controlling the dissolution or precipitation of a compound. As discussed above, the dissolution of FeS at alkaline pH is low. However, the dissolution of FeS at acidic pH can be enhanced, resulting in more sulfide present in solution (Wolthers et al., 2005b). When FeS co-exists with Sb(III) in solution, Sb(III) and Fe (II) may compete to be bound to the sulfide. The solubility product of $Sb_2S_3$ ($\log K_{sp} = -92.8$, Mane and Lokhande, 2003) is much lower than that of crystalline FeS ($\log K_{sp} = -27.39$, Jong and Parry, 2003) and that of nanoparticle FeS ($\log K_{sp} = -3.5$, Rickard, 2006), so Sb(III) has a higher potential than Fe(II) to be bound to the sulfide. According to the discussion above, the reaction between Sb(III) and FeS is proposed as follows.

$$3\ FeS_{(s)} + 2\ Sb(OH)_3 + 6\ H^+ \rightarrow 3\ Fe^{2+} + Sb_2S_{3(s)} + 6\ H_2O \quad (3)$$

This reaction has also previously been proposed by Han et al. (2018). This reaction is well consistent with the result of the kinetic experiment (FeS + Sb(III)) at pH 5. In this experiment, the concentration of FeS (Fig. 4a) was highly correlated ($R^2 = 0.89$) with that of $Sb(III)_{aq}$ (Fig. 4d), indicating a close relation between the partial dissolution of solid FeS and the decrease of aqueous Sb(III). The decrease of $Sb(III)_{aq}$ could be attributed to the formation of $Sb_2S_3$ because the TEM analysis showed the occurrence of $Sb_2S_3$ precipitates in the solid phases (Fig. 5). Subsequently, the theoretical stoichiometry between FeS dissolution and $Sb_2S_3$ precipitation was calculated. Because the decrease of FeS before 6 min was highly related to the effect of pH on the stability of FeS, the stoichiometry was calculated based on the variation of the concentrations of FeS and $Sb(III)_{aq}$ after 6 min. From 6 to 1,440 min, the FeS and $Sb(III)_{aq}$ (expressed as $Sb(OH)_3$ in reaction (3)) decreased from 19.84 to 11.91 mg/L to 11.42 and 3.65 mg/L, respectively. This is equivalent to a molar $FeS_{dissolution}$: $Sb(III)_{decrease}$ ratio of 1.401, which is close to the theoretical stoichiometry of $FeS_{dissolution}$: $Sb(III)_{decrease} = 1.5$ in reaction (3). Therefore, this ratio strongly suggests that reaction (3) occurred in the interaction of Sb(III) with FeS at pH 5. In this experiment, if the decreased $Sb(III)_{aq}$ mostly converted to $Sb_2S_3$ (i.e., the precipitation was much more significant than the adsorption of Sb(III)), it could be expected that 11.42 mg residual solid FeS co-existed with up to 11.54 mg $Sb_2S_3$ in the final solid phases of 1 L reaction mixture. However, no signals of $Sb_2S_3$ were detected in the XRD analysis (see

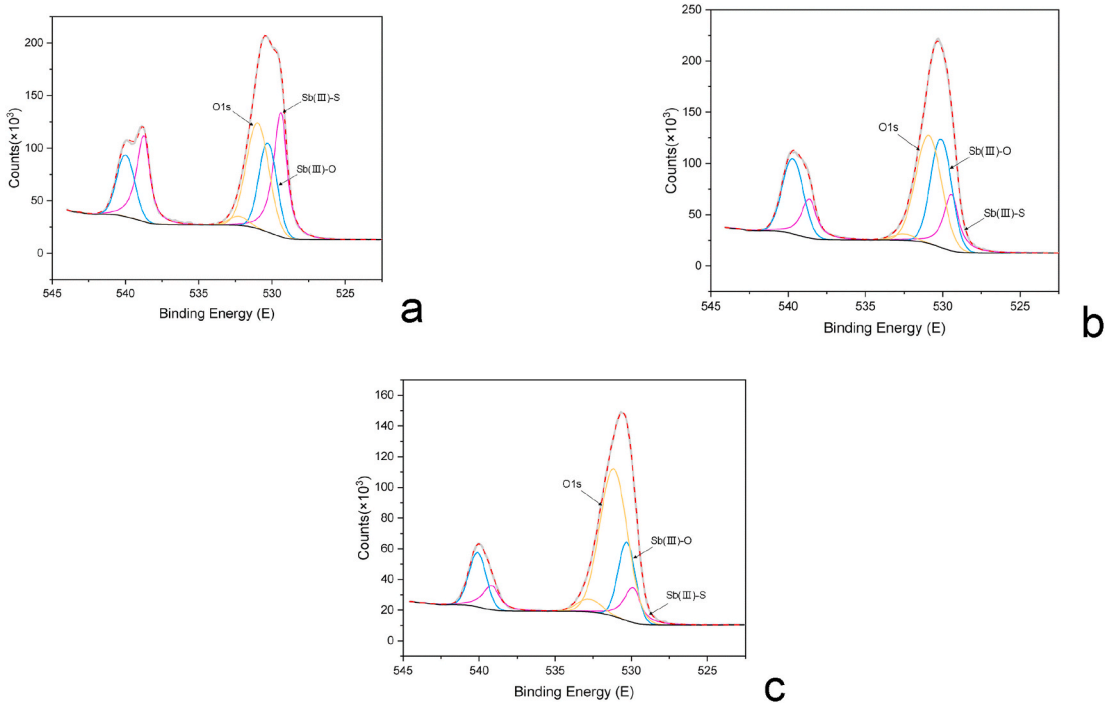


**Fig. 7.** XPS spectra of Sb 3d peaks for the solid phases after interaction (a: pH 5; b: pH 7.5; c: pH 9).

above). This possibly means that the precipitates of $Sb_2S_3$ were amorphous. Similarly, Han et al. (2018) also reported a poorly crystalline phase of $Sb_2S_3$ in the interaction of Sb(III) with FeS.

The precipitation of $Sb_2S_3$ was more significant at lower pH. This is consistent with the variation of $Sb(III)_{aq}$ concentration in both the equilibrium and the kinetic experiments. In the equilibrium experiments (FeS + Sb(III)) $Sb(III)_{aq}$ was much less at lower pH (Fig. 3), and in the kinetic experiments (FeS + Sb(III)) $Sb(III)_{aq}$ decreased more significantly when pH was lower (Fig. 4d). The TEM analysis on the solid phases of these experiments also revealed that precipitates of $Sb_2S_3$ were more frequently found at pH 5 compared to pH 7.5. The more precipitates of $Sb_2S_3$ at lower pH corresponded to the higher dissolution of FeS. This is consistent with the pH dependence of the solubilities of both $Sb_2S_3$ and FeS. As pH decreases, the solubility of $Sb_2S_3$ decreases significantly (Oslen et al., 2018) while the solubility of FeS increases significantly (Fig. 2).

In addition to the formation of $Sb_2S_3$, Sb in sulfidic systems has been reported to be able to form thioantimony species, e.g., $Sb_2S_4^{2-}$ and $HSb_2S_4^-$ (Polack et al., 2009; Planer-Friedrich and Scheinost, 2011; Ye et al., 2020). It has been reported that pH is a more significant factor compared to sulfide in controlling the transformation between $Sb_2S_3$ and thioantimonite (Chen et al., 2020). The solubility of $Sb_2S_3$ has been reported to decrease significantly with decreasing pH (Krupp, 1988; Olsen et al., 2018). In a study on the effect of pH on the transformation of aqueous Sb species in a sulfidic system, Chen et al. (2020) reported that, though in the presence of excess sulfide, $Sb_2S_3$ did not dissolve when pH was lower than 6.5 while significant dissolution of $Sb_2S_3$ through thiolation was triggered when pH increased to 6.5. It can be postulated that, in a sulfidic system, acidic pH favors the precipitation of $Sb_2S_3$ while alkaline pH favors the dissolution of $Sb_2S_3$ through thiolation with excess sulfide. This is similar to the formation of $As_2S_3$ that can be favored under acidic conditions (Wilkin and Ford, 2002; Rodriguez-Freire et al., 2014). Therefore, thioantimony species are likely to form only at high pH. However, due to the lack of excess sulfide in our system, it is assumed that the amount of thioantimony species was small and could not affect the dissolution of FeS significantly. This notion can be supported by the stable concentration of solid FeS over time in the kinetic experiment at pH 9 (Fig. 4c). The adsorption of thioantimony species on FeS is postulated to be weak, because the chemical behavior of Sb is comparable to that of As (Filella et al., 2002a; Casiot et al., 2007) and thioarsenates have been reported to have a lower affinity to FeS compared with arsenate and arsenite (Couture et al., 2013; Vega et al., 2017).

Regarding the mineral-water interaction, ion exchange is also a significant process that might occur at the mineral surface (Coles et al., 2000; Tertre et al., 2013). In the kinetic experiment (Fe(II)+Sb(III)) at pH 9, the concentration of FeS in the presence of Sb(III) was basically constant over time (Fig. 4c). This finding implies that exchange of Sb(III) for Fe(II) at the surface of FeS was not significant at alkaline pH. However, the effect of ion exchange under acidic and neutral conditions can not be identified.

Moreover, no precipitates of $Sb_2S_3$ were observed at pH 9 in the TEM analysis. This can be attributed to the low dissolution of FeS under alkaline conditions (Fig. 2). Therefore, the interaction of Sb(III) with FeS at pH 9 is considered to be dominated by Sb(III) adsorption. The adsorption of Sb(III) on the FeS particles can occur through functional groups on FeS. It has previously been suggested that the surface of FeS has two possible functional groups: an iron(II) hydroxyl functional group $\equiv FeOH^0$ and a sulfide functional group $\equiv SH^0$ (Bebie et al., 1998). In a previous study, Han et al. (2018) reported that Sb coordination with S was dominant at pH 5 while the contribution of Sb coordination with O increased at pH 9. Additionally, with increasing pH, more As(III) is bound to O (As–O) and form $\equiv Fe–OAs(OH)_2$, whereas with decreasing pH, more As(III) is bound to S(-II) in the form of $\equiv S_2–As(OH)$ (Gallegos et al., 2007). Because Sb usually shows a similar chemical behaviour to As (Filella et al., 2002a; Casiot et al., 2007), it is here proposed that Sb (III) was primarily bonded to O in the form of $\equiv Fe–OSb(OH)_2$ under alkaline conditions while it was primarily bonded to S(-II) in the form of $\equiv S_2–Sb(OH)$ under acidic conditions. In a study on the reduction of Sb (V) on the surface of FeS, Kirsch et al. (2008) suggested the Sb(III) coordination with S(-II) in a form of $SbS_3$ complex after Sb(V) was reduced to Sb(III).

## 4. Conclusions

The interaction of Sb(III) with FeS was found to be highly pH dependent. Under acidic and alkaline conditions, different mechanisms were found to significantly affect the interaction of Sb(III) with FeS particles. Generally, Sb(III) adsorption was the predominant process at high pH, whereas a mineral-replacement-like reaction (FeS replaced by $Sb_2S_3$) occurred at low pH, possibly due to the much lower solubility of $Sb_2S_3$ than that of FeS. The replacement of FeS by $Sb_2S_3$ was more significant at lower pH. Moreover, the replacement of FeS by $Sb_2S_3$ was a relatively slow process compared to the acidic dissolution of FeS.

In groundwater and anoxic sediments, FeS is an important metastable mineral that affects the mobility of metal(loid)s. This study improves knowledge about the interaction of Sb(III) with FeS in anoxic systems.

## Declaration of competing interest

The authors declare that they have no known competing financial interests or personal relationships that could have appeared to influence the work reported in this paper.

## Acknowledgements

This study was financially supported by the China National Key Research and Development Program (Nos. 2020YFC1807700 and 2017YFD0801000) and the China National Natural Science Foundation (No. U1612442).

## References

Amarasiriwardena, D., Wu, F., 2011. Antimony: emerging toxic contaminant in the environment. Microchem. J. 97, 1–3.
APHA, 1998. Standard Methods for the Examination of Water and Wastewater, twentieth ed. American Public Health Association/American Water Works Association, Baltimore, USA.
Ashley, P.M., Craw, D., Graham, B.P., Chappell, D.A., 2003. Environmental mobility of antimony around mesothermal stibnite deposits, New South Wales, Australia and southern New Zealand. J. Geochem. Explor. 77, 1–14.
Bebie, J., Schoonen, M.A.A., Fuhrmann, M., Strongin, D.R., 1998. Surface charge development on transition metal sulfides: an electrokinetic study. Geochem. Cosmochim. Acta 62 (4), 633–642.
Burton, E.D., Johnston, S.G., Bush, R.T., 2011. Microbial sulfidogenesis in ferrihydrite-rich environments: effects on iron mineralogy and arsenic mobility. Geochem. Cosmochim. Acta 75, 3072–3087.
Burton, E.D., Hockmann, K., Karimian, N., Johnston, S.G., 2019. Antimony mobility in reducing environments: the effect of microbial iron(III)-reduction and associated secondary mineralization. Geochem. Cosmochim. Acta 245, 278–289.
Casiot, C., Ujevic, M., Munoz, M., Seidel, J.L., Elbaz-Poulichet, F., 2007. Antimony and arsenic mobility in a creek draining an antimony mine abandoned 85 years ago (upper Orb basin, France). Appl. Geochem. 22, 788–798.
Chen, Y., Liang, W., Li, Y., Wu, Y., Chen, Y., Xiao, W., Zhao, L., Zhang, J., Lie, H., 2019. Modification, application and reaction mechanisms of nano-sized iron sulfide particles for pollutant removal from soil and water: a review. Chem. Eng. J. 362, 144–159.
Chen, J., Zhang, G., Ma, C., Li, D., 2020. Antimony removal from wastewater by sulfate-reducing bacteria in a bench-scale upflow anaerobic packed-bed reactor. Acta Geochim 39 (2), 203–215.
Coles, C.A., Rao, S.R., Yong, R.N., 2000. Lead and cadmium interactions with mackinawite: retention mechanisms and the role of pH. Environ. Sci. Technol. 34, 996–1000.
Couture, R.-M., Rose, J., Kumar, N., Mitchell, K., Wallschläger, D., Van Cappellen, P., 2013. Sorption of arsenite, arsenate, and thioarsenates to iron oxides and iron sulfides: a kinetic and spectroscopic investigation. Environ. Sci. Technol. 47, 5652–5659.

Csakberenyi-Malasics, D., Rodriguez-Blanco, J., Kis, V., Recnik, A., Benning, A., Posfai, M., 2012. Structural properties and transformations of precipitated FeS. Chem. Geol. 294–295, 249–258.
Fawcett, S.E., Jamieson, H.E., 2011. The distinction between ore processing and post-depositional transformation on the speciation of arsenic and antimony in mine waste and sediment. Chem. Geol. 283, 109–118.
Filella, M., Belzile, N., Chen, Y.-W., 2002a. Antimony in the environment: a review focused on natural waters I. Occurrence. Earth Sci. Rev. 57, 125–176.
Filella, M., Belzile, N., Chen, Y.-W., 2002b. Antimony in the environment: a review focused on natural waters II. Relevant solution chemistry. Earth Sci. Rev. 59, 265–285.
Fu, Z., Zhang, G., Li, H., Chen, J., Liu, F., Wu, Q., 2016. Influence of reducing conditions on the release of antimony and arsenic from a tailing sediment. J. Soils Sediments 16, 2471–2481.
Gallegos, T.J., Hyun, S.P., Hayes, K.F., 2007. Spectroscopic investigation of the uptake of arsenite from solution by synthetic mackinawite. Environ. Sci. Technol. 41, 7781–7786.
Gong, Y., Tang, J., Zhao, D., 2016. Application of iron sulfide particles for groundwater and soil remediation: a review. Water Res. 89, 309–320.
Han, Y.-S., Gallegos, T.J., Demond, A.H., Hayes, K.F., 2011. FeS-coated sand for removal of arsenic(III) under anaerobic conditions in permeable reactive barriers. Water Res. 45, 593–604.
Han, Y.-S., Seong, H.J., Chon, C.-M., Park, J.H., Nam, I.-H., Yoo, K., Ahn, J.S., 2018. Interaction of Sb(III) with iron sulfide under anoxic conditions: similarities and differences compared to As(III) interactions. Chemosphere 195, 762–770.
He, M.C., Wang, X.Q., Wu, F.C., Fu, Z.Y., 2012. Antimony pollution in China. Sci. Total Environ. 421, 41–50.
Jeong, H.Y., Lee, J.H., Hayes, K.F., 2008. Characterization of synthetic nanocrystalline mackinawite: crystal structure, particle size, and specific surface area. Geochem. Cosmochim. Acta 72, 493–505.
Jong, T., Parry, D.L., 2003. Removal of sulfate and heavy metals by sulfate reducing bacteria in short-term bench scale upflow anaerobic packed bed reactor runs. Water Res. 37, 3379–3389.
Karimian, N., Johnston, S.G., Burton, E.D., 2018. Iron and sulfur cycling in acid sulfate soil wetlands under dynamic redox conditions: a review. Chemosphere 197, 803–816.
Kirsch, R., Scheinost, A.C., Rossberg, A., Banerjee, D., Charlet, L., 2008. Reduction of antimony by nano-particulate magnetite and mackinawite. Miner. Mag. 72, 185–189.
Kulp, T.R., Miller, L.G., Braiotta, F., Webb, S.M., Kocar, B.D., Blum, J.S., Oremland, R.S., 2014. Microbiological reduction of Sb(V) in anoxic freshwater sediments. Environ. Sci. Technol. 48, 218–226.
Krupp, R.E., 1988. Solubility of stibnite in hydrogen-sulfide solutions, speciation, and equilibrium-constants, from 25 to 350 °C. Geochem. Cosmochim. Acta 52 (12), 3005–3015.
Mane, R.S., Lokhande, C.D., 2003. Thickness-dependent properties of chemically deposited $Sb_2S_3$ thin films. Mater. Chem. Phys. 82, 347–354.
Ohfuji, H., Rickard, D., 2005. Experimental syntheses of framboids - a review. Earth Sci. Rev. 71, 147–170.
Olsen, N.J., Mountain, B.W., Seward, T.M., 2018. Antimony(III) sulfide complexes in aqueous solutions at 30 °C: a solubility and XAS study. Chem. Geol. 476, 233–247.
Planer-Friedrich, B., Scheinost, A.C., 2011. Formation and structural characterization of thioantimony species and their natural occurrence in geothermal waters. Environ. Sci. Technol. 45, 6855–6863.
Polack, R., Chen, Y.-W., Belzile, N., 2009. Behaviour of Sb(V) in the presence of dissolved sulfide under controlled anoxic aqueous conditions. Chem. Geol. 262, 179–185.
Rickard, D., 1995. Kinetics of FeS precipitation: Part 1. Competing reaction mechanisms. Geochem. Cosmochim. Acta 59, 4367–4379.
Rickard, D., 2006. The solubility of FeS. Geochem. Cosmochim. Acta 70, 5779–5789.
Rodriguez-Freire, L., Sierra-Alvarez, R., Root, R., Chorover, J., Field, J., 2014. Biomineralization of arsenate to arsenic sulfides is greatly enhanced at mildly acidic conditions. Water Res. 66, 242–253.
Tertre, E., Hubert, F., Bruzac, S., Pacreau, M., Ferrage, E., Pret, D., 2013. Ion-exchange reactions on clay minerals coupled with advection/dispersion processes. Application to $Na^+/Ca^{2+}$ exchange on vermiculite: reactive-transport modeling, batch and stirred flow-through reactor experiments. Geochem. Cosmochim. Acta 112, 1–19.
Tighe, M., Lockwood, P.V., Ashley, P.M., Murison, R.D., Wilson, S.C., 2013. The availability and mobility of arsenic and antimony in an acid sulfate soil pasture system. Sci. Total Environ. 463–464, 151–160.
Ungureanu, G., Santos, S., Boaventura, R., Botelho, C., 2015. Arsenic and antimony in water and wastewater: overview of removal techniques with special reference to latest advances in adsorption. J. Environ. Manag. 151, 326–342.
Vega, A.S., Planer-Friedrich, B., Pasten, P.A., 2017. Arsenite and arsenate immobilization by preformed and concurrently formed disordered mackinawite (FeS). Chem. Geol. 475, 62–75.
Wang, H., Chen, F., Mu, S., Zhang, D., Pan, X., Lee, D.-J., Chang, J.-S., 2013. Removal of antimony (Sb(V)) from Sb mine drainage: biological sulfate reduction and sulfide oxidation-precipitation. Biores. Technol. 146, 799–802.
Wilkin, R., Ford, R., 2002. Use of hydrochloric acid for determining solid-phase arsenic partitioning in sulfidic system. Environ. Sci. Technol. 36, 4921–4927.
Wilson, S.C., Lockwood, P.V., Ashley, P.M., Tighe, M., 2010. The chemistry and behaviour of antimony in the soil environment with comparisons to arsenic: a critical review. Environ. Pollut. 158, 1169–1181.
Wolthers, M., van der Gaast, S.J., Rickard, D., 2003. The structure of disordered mackinawite. Am. Mineral. 88, 2007–2015.
Wolthers, M., Charlet, L., van Der Linde, P.R., Rickard, D., van Der Weijden, C.H., 2005a. Surface chemistry of disordered mackinawite (FeS). Geochem. Cosmochim. Acta 69 (14), 3469–3481.
Wolthers, M., Charlet, L., van der Weijden, C.H., van der Linde, P.R., Ricard, D., 2005b. Arsenic mobility in the ambient sulfidic environment; sorption of arsenic(V) and arsenic(III) onto disordered mackinawite. Geochem. Cosmochim. Acta 69, 3483–3492.
Xie, X., Pi, K., Liu, Y., Liu, C., Li, J., Zhu, Y., Su, C., Ma, T., Wang, Y., 2016. In-situ arsenic remediation by aquifer iron coating: field trial in the Datong basin, China. J. Hazard Mater. 302, 19–26.
Ye, L., Meng, X., Jing, C., 2020. Influence of sulfur on the mobility of arsenic and antimony during oxic-anoxic cycles: differences and competition. Geochem. Cosmochim. Acta 288, 51–67.
Zhang, G., Ouyang, X., Li, H., Fu, Z., Chen, J., 2016. Bioremoval of antimony from contaminated waters by a mixed batch culture of sulfate-reducing bacteria. Int. Biodeterior. Biodegrad. 115, 148–155.